Progress on emerging photocatalysts for treatment of dyes in wastewater: a review

Muhammad Syah Saifullah Osman[a], Nur Hashimah Alias[a,*], Nur Shafiqah Jamaluddin[a], Norfadhilatuladha Abdullah[b], Nur Hidayati Othman[a], Fauziah Marpani[a], Muhammad Shafiq Mat-Shayuti[a], Shareena Fairuz Abdul Manaf[a], Tutuk DjokoKusworo[c]

[a]*Department of Oil and Gas Engineering, School of Chemical Engineering, College of Engineering, Universiti Teknologi MARA, 40450 Shah Alam, Selangor, Malaysia, emails: nurhashimah@uitm.edu.my (N.H. Alias), muhammadsyahsaifullah@gmail.com (M.S.S. Osman), nurshafiqahjamaluddin96@gmail.com (N.S. Jamaluddin), nurhidayati0955@uitm.edu.my (N.H. Othman), fauziah176@uitm.edu.my (F. Marpani), shafiq5779@uitm.edu.my (M.S. Mat-Shayuti), shareenafairuz@uitm.edu.my (S.F.A. Manaf)*
[b]*Advanced Membrane Technology Research Centre (AMTEC), Universiti Teknologi Malaysia, 81310 Skudai, Johor, Malaysia, email: fadhilatuladha@gmail.com*
[c]*Department of Chemical Engineering, Faculty of Engineering, Diponegoro University, Semarang, 50275, Indonesia, email: tdkusworo@che.undip.ac.id*

ABSTRACT

Discharging of coloured dyes into wastewater has become one of the crucial issues around the world. Among various established alternatives to treat dye-contaminated water, photocatalytic degradation is a promising method to remove various dyes from water and wastewater due to their excellent photocatalytic activity and minimal final by-products. Nowadays, an immense number of photocatalysts have been synthesized and modified to achieve efficient treatment of photocatalytic degradation on dyes. On top of that, criteria include appropriate band gap energy of photocatalysts, applicability for solar light irradiation, good stability, and maximum recyclability have become the main prioritized. Herein, this review summarised the progress of emerging photocatalysts, graphene oxide, graphitic carbon nitride (g-C$_3$N$_4$) and molybdenum disulfide (MoS$_2$) in treating dyes. Furthermore, the performance of photocatalyst, the type of dyes treated, and significant findings from the treatment was also discussed. Finally, the future trends and challenges in applying photocatalysts to treat dyes in wastewater are comprehensively deliberated.

Keywords: Photocatalytic degradation; Photocatalyst; Wastewater; Dyes; Graphene oxide; Graphitic carbon nitride; Molybdenum disulfide

1. Overview on dye wastewater

The increase of industrial growth rate and human population have consumed natural resources faster than the ecosystem can generate. Therefore, industrial processes are one of the major consumers that lead to the deterioration of the global ecosystem and natural resources [1]. Other than that, water pollution caused by the discharge of wastewater from industrial and municipal has also captivated the researcher's attention to developing a sustainable and economical solution. It has been reported that agricultural industries primarily release about 70% of wastewater worldwide while the other 30% comes from municipal and other industries [2]. On average, high-income countries, the country that has a gross national income (GNI) per capita of more than $12,000, treat about 70% of their municipal

---

* Corresponding author.

and industrial wastewater they generated. However, for low-income countries, only 8% of them conduct wastewater treatment [3]. Due to the rising wastewater discharge, various organic pollutants are rising in water resources, such as pharmaceutical waste, pesticides and dyes. Among these, dyes in wastewater have become significant global attention because most of them are very persistent to degrade. The detection of various dyes in soils and aqueous environments has worsened the worldwide water resource's condition because it can threaten human beings, aquatic life, and all living organisms [1,4]. In particular, the release of dyes into the aquatic environment can reduce sunlight penetration and decrease dissolved oxygen concentration, producing anoxic conditions and subsequently posing a threat to aquatic life and public health [5]. Moreover, some synthetic dyes exhibit high biotoxicity, and higher toxic levels may result causing mutagenic, carcinogenic, and teratogenic effects on public health. Therefore, wastewater treatment technologies to eliminate dyes in wastewater have become a research focus.

Generally, dyes can be categorized into natural and synthetic/artificial dyes. Natural dyes originated from plant sources, including leaves, wood, roots, berries, bark, fungi, and lichens, while artificial dyes could be synthesized from chemicals, earth minerals and petroleum derivatives [6]. Synthetic dyes can be classified into two distinct reported groups: anionic and cationic dyes. Anionic dyes consist of three types of dyes: direct dyes, acid dyes, and reactive dyes. Acid dyes are water-soluble anionic dyes carrying organic sulphonic and carboxylic acid groups (SO_3H and $COOH$). Typically, these dyes are widely applied in the textile, pharmaceutical, printing, and paper industries due to their bright colour and high solubility [7]. Reactive dyes form a covalent bond with amine or sulfhydryl protein groups in textile fibres. It has been reported that reactive dyes are the most used dyes because of their high wet fastness, brilliance, and wide range of hues. Congo red dye is the first direct dye discovered in 1884 [8]. Direct dyes are soluble when applied from the aqueous medium in electrolyte and have a high affinity for cellulosic fibres. Commonly, direct dye is used in the dyeing of cotton, rayon, paper, leather, and to some extent, nylon. Other anionic dyes used extensively as a model in adsorption and photodegradation are Alizarin red S, Methyl blue, Nuclear fast red, Sunset yellow FCF, Alizarin green, Methyl orange, Reactive black 5 and Acid red 73.

Cationic dyes are usually basic and positively charged and commonly called basic dyes. This dye is usually synthetic that act as bases, and when made soluble in water, they form a coloured cationic salt, which can react with the anionic sites on the surface of the substrate. As for tint firmly with bright shade and react faster on acrylic fibre than anionic or non-ionic dye, this type of dye is commonly used in textile industries [9]. Among basic dyes, the Methylene blue (MB) is the most used dye for industries very popular dye with extensive use. However, several health problems are associated with these dyes, such as high blood pressure, vomiting, diarrhoea, gastrointestinal pain, and dizziness [10]. MB has been used as a safe aquarium disinfectant and used to treat ammonia and nitrite poisoning in the aquarium. However, it will damage the plants and aquatic life in the aquarium if the dose used exceeds the concentration level limit.

Furthermore, Rhodamine B and Malachite green are also included in this group of dyes which can cause harmful effects to human health. Therefore, the control of water pollution caused by cationic dyes needs to be noticed before it becomes critical and uncontrollable. The general information of different dyes is tabulated in Table 1.

Depending on the influent's water quality and the effluent discharge standard, the water treatment process is operated through the combination of various water treatment facilities. Generally, several physicals, chemical, and biological treatment methods can be utilized for treating the dye contaminated wastewater in which each method has its advantages and disadvantages, respectively. For chemical-based treatment, coagulation–flocculation is recognized as a remarkable treatment method for treating industrial dye wastewater due to its simplicity and effectiveness in reducing pollutants in terms of turbidity, colour, and odour of wastewater. Nevertheless, this method becomes unattractive due to high energy demand, chemical reagents, and the generation of secondary sludge pollutants that require additional operational costs [18].

On the other hand, conventional biological treatment processes for textile wastewater significantly reduce chemical oxygen demand (COD). The advantages of the biological treatment process are their low operating cost, and pollutant mineralization is the advantage of the biological treatment method [19]. But the process does not have acceptable efficiency in high soluble dyes removal and COD removal [19]. Alternatively, a physical wastewater treatment method such as membrane separation technology and adsorption can give satisfactory efficiency of dyes removal. In the past years, membrane separation technology has attracted significant attention in water and wastewater treatment. In a direct membrane filtration system, several driving forces drive membrane application in wastewater treatment: pressure-driven, osmosis-driven, thermal-driven, and electrical-driven. However, most of the application of direct membrane filtration in treating dye contaminated water is mainly limited by membrane fouling [20].

On the other hand, adsorption demonstrates the advantages of low cost and simple operation [21]. Therefore, various adsorbents have been investigated to remove dyes in wastewater. However, the amount of adsorption sites reduces as the concentration increases, and thus the adsorption performance becomes slower. On top of that, the ability of adsorbents to regenerate in repeating cycles is also crucial to ensure an efficient adsorption performance.
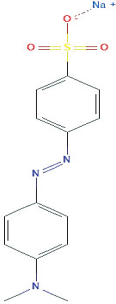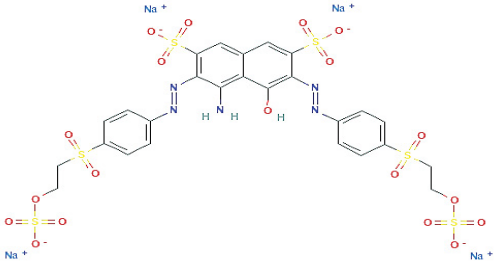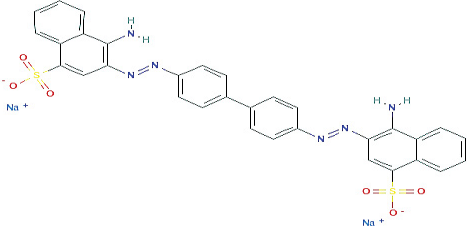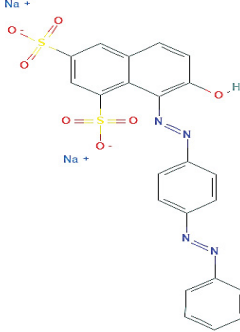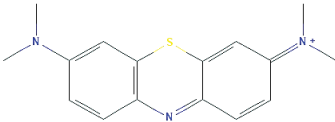
Recently, the photocatalytic degradation method has been regarded as promising in treating wastewater based on advanced oxidation processes (AOPs) due to their excellent reusability and higher efficiency in removing persistent dyes in wastewater [22–25]. Hong Wu et al. [13], previously implemented the photodegradation reaction of Methyl orange (MO) dye by using cuprous oxide (Cu_2O) combined with zinc aluminium (ZnAl) layered double hydroxides (Cu_2O/ZnAl-CLDH composite). Based on this study, ratio and temperature play a significant role in determining the performance of the CLDH composite. The ideal ratio to acquire a 90% photocatalytic degradation of MO is at a molar ratio of 1:1 (Cu:CLDH), calcined at 500°C. A low amount of CLDH may result in the unfavourable performance of composite,

Table 1
General data of various dyes and their molecular structure

Type of dye	Dye (Abbreviation)	Molecular weight (g mol^{-1})	Molecular structure	Reference
Anionic dye	Alizarin red S (ARS)	342.26		[11]
	Methyl blue (Aniline blue, AB)	799.80		[11]
	Nuclear fast red (NFR)	357.28		[11]
	Sunset yellow FCF (SY)	452.37		[11,12]
	Alizarin green (AG)	622.58		[11]

(Continued)
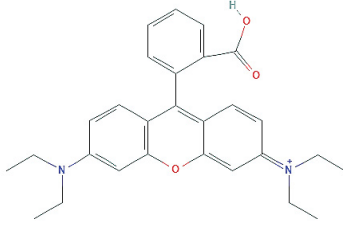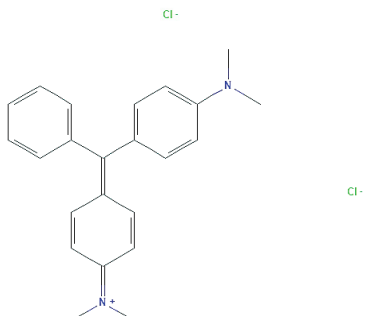
Table 1 Continued

Type of dye	Dye (Abbreviation)	Molecular weight (g mol⁻¹)	Molecular structure	Reference
Anionic dye	Methyl orange (MO)	327.33		[11,13]
	Reactive black 5 (RB5)	991.80		[14]
	Congo red (CR)	696.70		[8,12,15]
	Acid red 73 (AR)	556.51		[7]
Cationic dye	Methylene blue (MB)	319.85		[16]

(Continued)

Table 1 Continued

Type of dye	Dye (Abbreviation)	Molecular weight (g mol⁻¹)	Molecular structure	Reference
	Rhodamine B (RhB)	479.02		[17]
Anionic dye				
	Malachite green (MG)	364.91		[9]

and the excess amount of CLDH may cause the recombination of photogenerated electrons hole. Cu$_2$O/ZnAl-CLDH composite photocatalyst showed good reusability and stability for photodegradation of MO even after three cycles. The high removal efficiency has also been proved by Zhou et al., [14], who reported studies about the degradation of anionic dyes through photocatalytic activity. Synthesized CuO/ZnO composites using the *Penicillium corylophilum* cell to remove MB dyes. 97% of MB is removed from the sample after irradiation under the visible light within 85 min. Thus, many studies investigated the potential nanomaterials based photocatalyst on the degradation of dyes. This review discussed several potentials of the recent photocatalyst. Consequently, the current progress of highly potential photocatalysts for dye removal was further discussed in detail. The challenges and perspectives on the photodegradation performance of dyes were also included.

2. Photocatalytic degradation of dyes

In photocatalysis, the photocatalytic materials undergo photoexcitation by UV, visible or near infrared light depending on their energy band gaps and inactivate a wide range of waterborne microbes through a simple photocatalytic redox mechanism [26]. They utilized solid oxidizing species produced *in situ*, such as hydroxyl radicals (OH), to trigger a sequence of reactions that decomposes organic compounds having one or many double bonds into smaller and less harmful substances. The purpose of AOPs is to decrease the toxicity and hazardous compounds in the wastewater to the desired concentration before being safely discharged into water streams [4]. In other words, photocatalyst converts solar energy into chemical energy and thus degrades

harmful pollutants into non-toxic compounds. In particular, the general photocatalytic process usually involves three specific steps: charge generation, separation, and consumption [27]. As shown in Fig. 1, the photocatalyst is initially excited in the presence of light, and then, the electron–hole pairs on the valence band (VB) are separated. Then, the electrons are excited onto the conduction band (CB), leaving a hydrogen ion hole on the VB. Finally, the charge carriers are separated to the surface of the photocatalyst and participate in the redox reaction. The electron can reduce typical electron acceptors such as O$_2$ and H$_2$O to produce a reactive oxygen species on the photocatalyst surface. Simultaneously, the holes on the surface of the photocatalyst are recombined

Fig. 1. Schematic illustration of photocatalytic activity of a photocatalyst [28].

with the donor species, resulting in the mineralization of organic pollutants. In the photodegradation of dyes, the hole generated will act as the oxidizing agent and help form the mineralization products. At the same time, the hydroxyl radicals will undergo oxidation with the pollutant component and thus eliminate it from the wastewater.

Over the last decades, titanium oxide (TiO_2) nanomaterials attracted the most attention for dyes degradation because of their high reactivity, non-toxicity, physical and chemical stability. Its high activity originates from the efficient generation of charge carriers (hole [h^+] and electron [e^-]) upon UV light irradiation (band gap of 3.2 eV) and relatively good separation of the carriers, such as holes either free or trapped hydroxyl radicals ($^•OH$), superoxide anions (O^{2-}) and singlet oxygen among others [29]. Initially, the excellent performance of TiO_2 was discovered by Fujishima and Honda (1972) when polluted water was irradiated with UV using a TiO_2 electrode. They successfully discovered that the contaminant in the polluted water could be degraded to a less toxic substance through photochemical decomposition under irradiation of light [30]. Nowadays, converting solar energy into chemical energy has attracted numerous scientists researching the photocatalysis field. Therefore, identifying a highly photoactive photocatalyst with high light utilization efficiency focuses on photocatalysis research. Nevertheless, TiO_2 suffers from several drawbacks, such as the narrow scope of solar energy absorption and fast recombination of photo generated carriers, which decreased its photocatalytic activity. Therefore, many efforts were made to deal with this issue by modifying the pristine TiO_2 and investigating other potential nanomaterials for the degradation of dyes.

Fouda et al. [31], reported titanium dioxide/zeolite Socony Mobil-5 (TiO_2/ZSM-5) composite for Reactive black 5 (RB5). The degradation of azo-dye, Reactive black 5 (RB5) was investigated in the presence of titanium dioxide (TiO_2)/ zeolite Socony Mobil-5 (ZSM-5), and the result showed that 95% degradation efficiency was obtained after 10 min of exposure towards TiO_2/ZSM-5 at a neutral pH and in a room temperature. Another study reported on the synthesis of Fe_3O_4@SiO_2 coated with the g-C_3N_4/TiO_2 composite at the outer shell. It was found that the utilization of photons from sunlight is higher in the Fe_3O_4@SiO_2@C_3N_4/TiO_2 composite compared to the TiO_2/Fe_3O_4 composite. The highest reaction rate constant of composite for the degradation of Rhodamine B (RhB) is achieved at 10% wt. of composite [32].

In recent years, several excellent nanomaterials with satisfactory band gap and recombination rates such as graphene oxide (GO), graphitic carbon nitride (g-C_3N_4), and molybdenum disulfide (MoS_2) has been discovered and widely applied to remove organic pollutant in wastewater because of their excellent (structure/properties). Some researchers have also constructed a composite photocatalyst by incorporating other materials in the photocatalyst, for example, magnetic materials.

The magnetic composite carrier can distribute photocatalyst, which is not exposed to light inside the original catalyst on the surface of the magnetic carrier, thus increasing the effective photocatalytic reaction area. Furthermore, the introduced magnetic carrier can effectively lower the photocatalyst content without decreasing the total performance because photooxidation only occurs at the photocatalyst surface [33]. For example, Sudhaik et al. [34] reported the use of nickel ferrite ($NiFe_2O_4$) loaded with graphitic carbon nitride (g-C_3N_4) to degrade oxytetracycline from wastewater under solar light. They observed that the catalytic efficiency of bare ($NiFe_2O_4$) is reduced due to the agglomeration of magnetic nanoparticles. At the same time, the recovery of the non-modified g-C_3N_4 from reaction solution required approximately 8 h by using a simple sedimentation process. However, compared to the g-C_3N_4 loaded with nickel ferrite, the recovery time shortened to 2 min, and it can be used consecutively in ten catalytic cycles. This study demonstrates that the utilization of magnetic property lowers the separation cost and can also shorten the recovery time of photocatalyst from the reaction solution compared to the use of non-modified photocatalyst [35]. Further detailed discussion on various aspects of the potential nanomaterials as single and composite photocatalyst for degradation of dyes.

3. Synthesis of potential photocatalysts for dye degradation

3.1. Graphene oxide

Graphene oxide (GO) is currently one of the most promising advanced nanomaterials in photocatalysis. Generally, GO is the derivative of graphene. GO can be utilized as a stand-alone photocatalyst, co-catalyst in the composite, or support material or semiconductor catalysts [36]. The structure of graphene and GO is displayed in Fig. 2. Graphene consists of a carbon atom with a single-atom-thick sheet
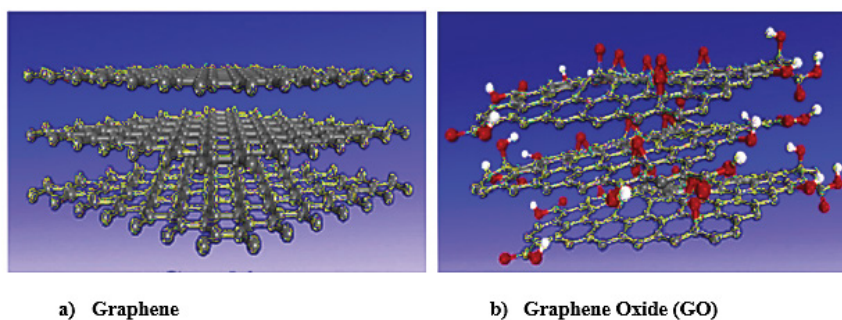

a) **Graphene** b) **Graphene Oxide (GO)**

Fig. 2. Structures of (a) graphene and (b) graphene oxide [46].

arranged in a hexagonal arrayed sp^2 structure [37]. GO consists of a single layer of graphite oxide produced through facile chemical treatment of graphite by oxidation, followed by the exfoliation processes in water or organic solvents [38]. Another established method to form GO sheets is modified Hummers [39–44]. Generally, GO is composed of carbon atoms, arranged in a hexagonal lattice, and decorated with oxygen functional groups (OFG) on their basal plane defects either the epoxy or the hydroxyl groups, C–O and at the layer's edges (carboxyl groups, O=C–O). The broad range of OFG anchored on both basal planes and edges of GO makes it vulnerable to exfoliate and functionalized well to yield a well-dispersed solution of individual graphene oxide sheets either in the water or in the water the organic solvents [45]. The GO monolayers can be deposited onto the surface of numerous substrates by controlling their density, thus allowing the production of thin conductive films on solid and flexible substrates, which enhances its use as composites. Many researchers have used GO as a precursor material for graphene-based composites.

Hu et al. [47], previously synthesized a composite based graphene oxide (GO) with non-peripheral octamethyl-substituted copper(II) phthalocyanine (GO/N-CuMe$_2$Pc) by using the ultrasonic method. They observed little Cr(VI) reduction when the Cr(VI) was introduced to pure GO or N-CuMe$_2$Pc, subjected to visible light irradiation. In contrast, in the presence of the GO/Pc composite, the rate of photocatalytic reduction of Cr(VI) increased up to 95% in the sample solution. Furthermore, it is described that the GO sheets are a very good acceptor for the excited electron of N-CuMe$_2$Pc. Thus, the introduction of GO sheets significantly affects the composite's light absorption and charge separation behaviour by slowing down the recombination rate of excited charge carriers.

Moreover, a recent study reported on the preparation of immobilized GO with BiOl/Fe$_3$O$_4$ through a simple coprecipitation method [48]. They analyzed the magnetic properties of the synthesized photocatalyst by using atomic force microscopy (AFM), and it is shown that the BiOl/Fe$_3$O$_4$@GO exhibited good dispersibility and stability. Furthermore, the magnetic saturation value of the photocatalyst is 23.0 emu g^{-1}, and the photocatalyst could be separated from the reaction solution approximately in 2 min by placing a magnet near the bottle sample. This quick separation of BiOl/Fe$_3$O$_4$@GO photocatalyst is suitable for its applicability in the slurry type photoreactors. In summary, the GO can be a suitable medium as a support material for efficient photocatalyst and as their promoter owing to its unique physicochemical properties, large specific surface and excellent optical transmittance.

3.2. Graphitic carbon nitride (g-C$_3$N$_4$)

Graphitic carbon nitride (gCN or g-C$_3$N$_4$) has been considered as an emerging metal-free photocatalyst for photodegradation of organic pollutants due to its low cost, non-toxicity, high stability and suitable band gap (2.7 eV) [23,24,49–52]. Fig. 3 shows the illustration formation of g-C$_3$N$_4$ from various precursors under heating treatment. Melamine and urea are the most typical materials precursor for the production of g-C$_3$N$_4$. The synthesized g-C$_3$N$_4$ absorbs solar photons of their energies, covert them into chemical energy, and subsequently perform photocatalytic degradation on hazardous organic pollutants to form harmless compounds [53]. The application of g-C$_3$N$_4$ has emerged in photocatalysis due to its unique nature, low toxicity, high chemical stability, and appropriate band gap energy [54]. However, quick recombination of excited charges and low surface area has limited its efficiency as it produced relatively poor performance in visible light absorption. Recently, various strategies have been applied to enhance the photocatalytic efficiency of g-C$_3$N$_4$, including doping with other
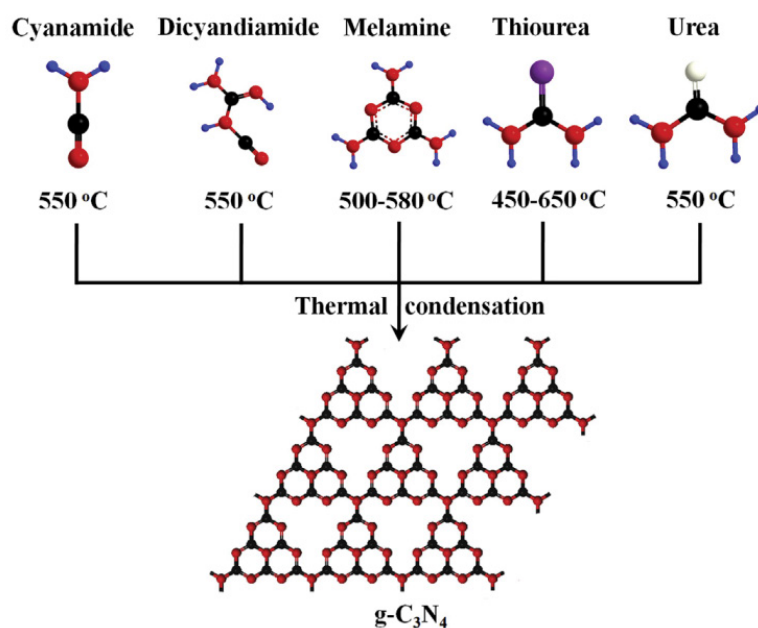

Fig. 3. Formation of g-C$_3$N$_4$ from various precursors under heating treatment [56].

transition metals or noble metals, non-metal doping and surface modification. It is due to the ability of electrons captured by these noble metallic ions, around which the photogenerated electron aggregate, giving rise to a higher separation of photogenerated electrons and holes [49]. However, the primary weakness of the photocatalyst is not the absorption of a sufficient proton to induce electronic excitation and create electron-hole pairs, but the separation of electrons from holes to comply with the required photocatalytic process is the primary step during photocatalysis. Therefore, the modification of g-C_3N_4 through foreign doping and constructing a hetero-junctional interface between g-C_3N_4 and neighbour semiconductors as the second semiconductor is needed to improve the charge separation process [55].

Most importantly, the light absorber's conduction band (CB) should be well above the conduction band of the sink semiconductor to induct and transport maximum charge density. Compared to most semiconductors, the conduction band of the g-C_3N_4 is well above. Hence, it is suitable to form a heterojunction with many semiconductors to obtain better properties and performances of photocatalytic degradation on dye pollutants.

An effective modification method for extending optical absorption of the graphitic carbon nitride is the introduction of noble metals. Doping or loading of these metals has been proven to generate more visible light absorption and improved charged separation. Viet et al. [49], have synthesized Ag-doped graphitic carbon nitride (g-C_3N_4) photocatalyst via a simple thermal condensation method. They used oxytetracycline (OTC) as their model pollutant. Through his research, it has been found that 7% of Ag loading onto the g-C_3N_4 showed the highest photocatalytic degradation efficiency of OTC, which is 98.7%. Moreover, he also stated that under optimal conditions, the OTC degradation rate is still constant at 85.6% even after seven consecutive runs, indicating the satisfactory stability and reusability of the photocatalyst. Besides that, Zhao et al. [57] decorated a ternary hybrid photocatalyst consisting of boron-doped graphitic carbon nitride with reduced graphene oxide (g-C_3N_4/rGO/boron) through a facile one-pot hydrothermal process. The energy-dispersive X-ray spectroscopy and X-ray photoelectron spectroscopy analysis indicate that the boron element is successfully incorporated in the composite at the peak of 192 eV. The dispersion of the boron element on the composite surface enhanced the photocatalytic of the ternary photocatalyst as the boron restricted the recombination of electron-hole pairs in the composite.

3.3. Molybdenum disulfide (MoS₂)

Nowadays, the utilization of molybdenum disulfide (MoS_2) as a photocatalyst for the degradation of pollutants has risen due to its excellent performance in photoelectric properties. The MoS_2 electronic band can be tuned with an indirect or direct band gap of 1.2 to 1.9 eV, determined by their number of layers [58]. The narrow band gap of the MoS_2, which is 1.29 eV, has enriched MoS_2 with photoelectrical effects, making MoS_2 a promising candidate in photocatalytic applications under visible light irradiation. Furthermore, due to the sizeable band-edge excitation of the metal centred d–d transition, the MoS_2 can possess an

electrocatalytic activity thanks to its unique electronic features. The properties and structure of MoS_2 are pretty similar to graphene. Both are n-type semiconductor materials [50], where the charge carriers in the crystal are mainly negative electrons. MoS_2 structure consists of Mo atom sandwiched between two S atoms and forms a two-dimensional layer. This layer can be multiple layers bonded by strong covalent bonds, and each layer is connected by weak Van der Waals force [59]. Generally, MoS_2 has three types of crystal structures which are the triangular prism structure (2H), hexahedron structure (Fig. 4a), and octahedron structure (Fig. 4b) [60]. Among these structures, the 2H-MoS_2 is the best crystal structure to be utilized as a photocatalyst because it has better stability under normal conditions. Besides that, the MoS_2 has a great range of wavelengths to absorb visible light photons, which is very advantageous for carrier separation. It is reported by Chen et al., [59] that photocatalytic activity of MoS_2 is enhanced when it is intercalated with a zinc aluminium hydrotalcite (ZnAl-LDH). The result from the Brunauer–Emmett–Teller analysis in his research shows that the small structure of the ZnAl-LDH pore has exposed more contact surface for MoS_2, which significantly impacts the adsorption capacity of target pollutants.

Furthermore, due to the large band-edge excitation of the metal-centred d–d transition, the MoS_2 can possess an electrocatalytic activity thanks to its unique electronic features. Similarly, MoS_2 often undergoes modification before being used as the photocatalyst and combined with other semiconductors with the band gap value lower than MoS_2 to increase their light-responsive ability and minimalize electron-recombination potential. Many researchers have carried out the performance of MoS_2 photocatalyst in treating the contaminant in the wastewater. To enhance the separation of MoS_2 from the contaminated solution and increase the recyclability of photocatalyst, they combine it with metal., For instance, Sun et al. [61] prepared the Ag-MoS_2 composite photocatalyst in the lab and tested it for reduction of chromium(VI) to chromium(III). Chromium(VI) purification is needed since this chemical has been listed as one of the toxic heavy metals and most common pollutants from industrial effluent. According to their research, in the dark condition, the redox reaction occurs as the Ag-MoS_2 photocatalyst acts as an electron donor through its self-oxidation. At the same time, the chromium(VI) anions work as electron acceptors. In terms of recyclability of the photocatalyst, the photocatalytic efficiency of chromium(VI) reduced after being used for the fourth time due to the change of MoS_2 structure.

3.4. Composite-based photocatalysts

Various methods have been reported to synthesize the composite photocatalyst, including hydrothermal, solvothermal, chemical precipitation and microwave assist methods. The most common and facile methods to prepare composite photocatalysts are hydrothermal, solvothermal, and chemical precipitation methods. In a hydrothermal method, temperature and pressure are the crucial parameters to produce a good quality photocatalyst. In a study by [62], they synthesized a hybrid ZnO-GO composite photocatalyst using hydrothermal method. First, the synthesized
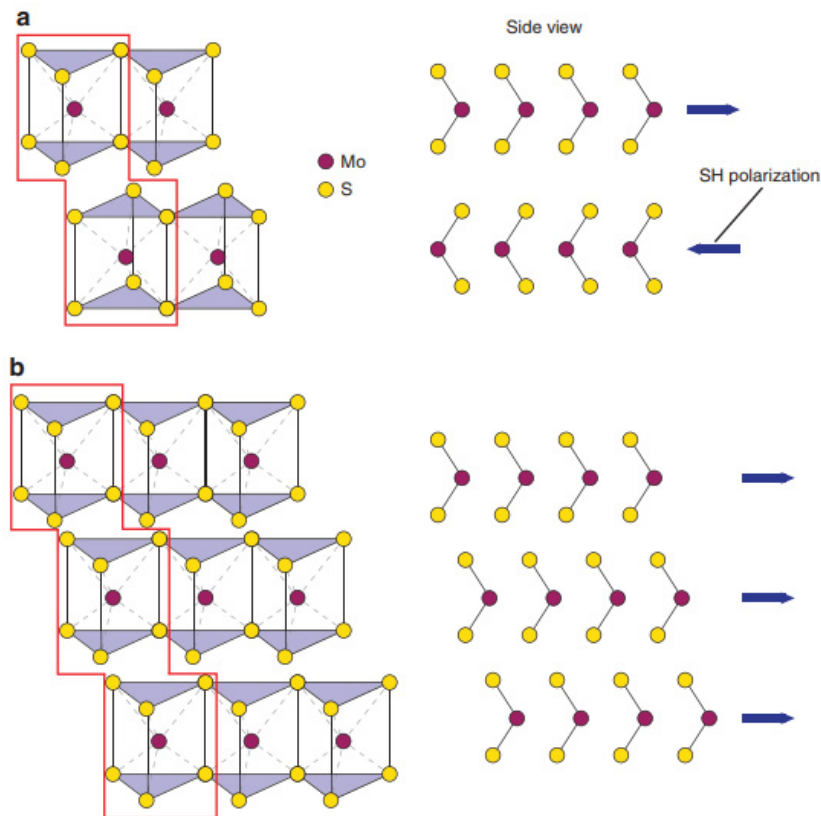
Fig. 4. Molecule structure of (a) 2-H MoS_2 (hexagonal) with trigonal geometry and (b) 1-T MoS_2 (tetragonal) with octahedron geometry [60].

GO has added to ZnO colloidal suspension with vigorous stirring for 2 h. After that, the mixture was sonicated for 30 min. Later, the mixture was transferred into a Teflon-lined autoclave and heated in the oven at 200°C for 12 h for hydrothermal reaction. After the reaction, the product was cooled down and subsequently washed for few times. Finally, the washed mixture was centrifuged and dried at 60°C for 24 h in an oven to obtain composite photocatalyst powder.

Similarly, Tong et al. [63] synthesized GO/g-C_3N_4 photocatalysts by adding 16 in 4 mg L^{-1} GO mixture and consequent with solution reaction-based method. On the other hand, some researchers developed composite photocatalyst using a two-step hydrothermal method to obtain excellent photocatalyst properties. Two steps of hydrothermal synthesis were commonly applied to remove traces of undesired species [64]. For example, the ZnO composite was prepared by a two-step hydrothermal method [65]. Initially, ZnO composite was washed with deionized water first, and then the mixture was suspended in 0.001 M $Zn(NO_3)_2$/0.05 M NaOH under magnetic stirring at 70°C for 2 h.

The solvothermal method is a standard procedure to develop composite photocatalyst [66,67]. Generally, the solvothermal method is quite similar to the hydrothermal method as reactants in both methods were placed in an autoclave containing water or organic compound. The reaction was carried out under high-temperature conditions. The difference between these processes is that the solvothermal method used non-aqueous solvent, whereas the

hydrothermal method used water as a reaction medium [68]. Hong Wu et al. [66] prepared g-C_3N_4/GO/MoS_2 photocatalyst via a solvothermal method. Acetic acid and cetyltrimethylammonium bromide were used as reaction mediums in the synthesis procedure, as depicted in Fig. 5. The synthesized composite photocatalyst exhibited a high transfer performance of photogenerated electrons.

Besides the thermal method, the chemical precipitation procedure is also an established method for preparing composite photocatalysts. It is also highlighted as a simple method without requiring further treatment under high pressure or temperature. As an example, in the preparation of ZnO/g-C_3N_4 composite photocatalyst, 250 mL of the zinc acetate solution were added dropwise into g-C_3N_4, under vigorous stirring, yielding a pale-yellow precipitate. The obtained residue was then washed with deionized water and ethanol. The resulting powder was then dried [69].

Furthermore, another study reported the preparation and effectiveness of Ag_3PO_4/GO/gC_3N_4 composite photocatalyst via chemical precipitation method for photodegradation of RhB dye under visible light irradiation [70]. Recently, the microwave-assisted method was also employed to synthesize composite photocatalyst to achieve high purity of photocatalyst. In addition, the synthesis process of the microwave-assisted method is also economical, simple and environmentally friendly [71]. Therefore, due to their facile process, composite photocatalyst can successfully be prepared within a short duration [72].
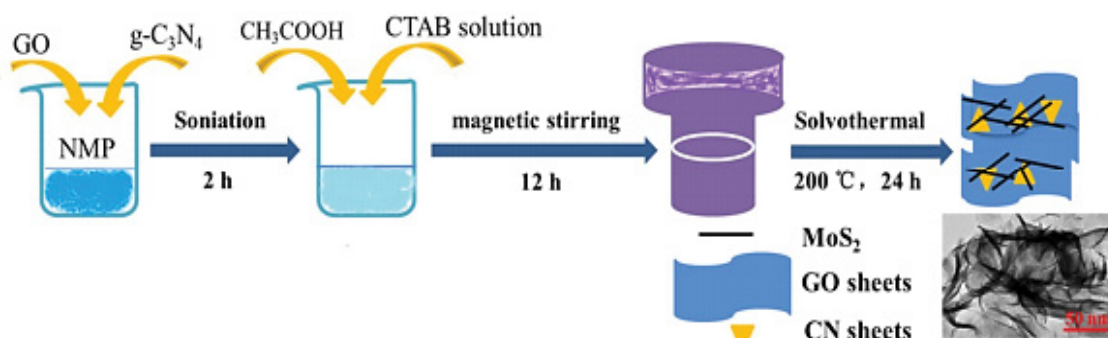
Fig. 5. Preparation of C_3N_4/GO/MoS_2 photocatalyst via solvothermal method [66].

4. Performance of photocatalysts on dyes degradation

This section emphasized the performance of three different types of photocatalyst, which are graphene oxide (GO), the graphitic carbon nitride (g-C_3N_4), and the molybdenum disulfide (MoS_2) towards dye degradation. These three photocatalysts have received significant attention in recent photocatalysis studies due to their unique properties and impressive performances. Furthermore, the intrinsic property of these photocatalysts has encouraged the researcher to combine it with other materials to increase their performance and rate of recycling of photocatalyst.

4.1. Performance of graphene oxide photocatalyst

GO is also a promising semiconductor photocatalyst that has been working on photodegradation of dyes by the researcher for the past few decades due to the vast functional groups of GO that act as anchoring sites for the various component. The functional groups mostly lay on the basal planes or at the edge of GO, and it consists of four functional groups: carboxyl, carbonyl, epoxide, and hydroxyl. The oxygenated groups in GO usually affect the electrical and mechanical properties of GO. It is reported that the electrical conductivity of GO is 64 ms m^{-1}, and the conductivity is stable over a wide range of temperatures. To assist the photocatalytic activity, GO is reliable since it has an effective π–π bond [45] and a smaller band gap than it acts as a photosensitizer [36]. The delocalized π bonds in the conjugated sp^2 bonded network on the carbon lattice with the resultant unsettled spacious of electronic π bonds increase thermal, electrical conductivity and inhibit the charge recombination of the graphene composites. Besides that, GO can extend the light absorption wavelength until the visible light region due to the smaller band gap. The extending of wavelength improved the charge transport when the GO combined with the heterogeneous photocatalyst, and it also increased the surface absorption of visible light. Thus, the photodegradation of dyes become more efficient.

A stand-alone GO photocatalyst has shown excellent results in various dye degradation such as Congo red (CR), RhB and MB [73]. Kumar and Kumar [74] reported that the synthesized GO could accelerate the degradation of MB dyes under light irradiation. It is due to the generated electron–hole pairs from p–p* excitation in the p-conjugated sp2 domains of GO after photon energy absorption [39].

Furthermore, Govindan et al. [75] synthesized GO photocatalyst via advance Hummer's route. The synthesized photocatalyst exhibit GO photocatalyst exhibits excellent TOC reduction of MO. Based on the study, photocatalytic irradiation time plays the most significant factor for MB degradation. However, several studies have shown that pristine GO is not photoactive enough to photodegraded several types of dye because of the rapid recombination of photogenerated charge carriers [73]. In this regard, many efforts have been made to synthesize GO composite for improving the photodegradation of dye performance using GO. Besides that, many research groups have reported the fabrication of some GO-based semiconductor materials to improve photocatalytic activities significantly to design some type-II heterojunctions or Z-scheme photocatalysts by coupling GO with GO various materials [62].

Khurshid et al. [73] successfully doped GO with transition metal elements including Co, and Ni, respectively, via the chemical precipitation method. The synthesized composite photocatalyst was used in the photodegradation of MO under ultraviolet light irradiation. The photocatalytic performance of Co and Ni-GO towards MO displayed higher degradation efficiency than pristine GO with photocurrent generation of 64.9 and 54.4 μA cm^{-2}, respectively. Besides metal elements, semiconductor nanoparticles have been widely used to prepare GO composite photocatalyst. Similarly, the chemical precipitation method synthesized highly ZnO-GO composite for photocatalytic performance under visible light [76]. The successful incorporation and homogeneous dispersion of ZnO were confirmed with transmission electron microscopy (TEM) analysis. The study also revealed that the synthesized photocatalyst exhibited high degradation efficiency against RhB. On the other hand, Das et al. [77] have successfully studied the photodegradation of CR using GO-CdSe quantum dots composite photocatalyst. The composite photocatalyst exhibited 90% degradation efficiency of CR under sunlight within 60 min.

On the other hand, Kamalam et al. [78] have successfully synthesized vanadium pentoxide (V_2O_5) nanorods/graphene oxide (GO) nanocomposite as an efficient photocatalyst under direct solar light-driven photocatalyst for the degradation of Victoria blue (VB) dye. Based on the study, they have found that the nanocomposite's band gap was reduced compared to pure GO and V_2O_5. On top of that, they have observed almost complete degradation (97.95%) of Victoria blue (VB) dye under direct sunlight illumination

within just 90 min. This was due to the excellent transfer of interfacial charge and the suppressed recombination of charge-carrier of this composite photocatalyst. To conclude, the combination of GO with other photocatalytic materials have extremely improved its photocatalytic ability, thus significantly enhancing the photocatalytic degradation performance on dye removal. Table 2 shows the summary of synthesized GO-based photocatalyst for dye removal.

4.2. Performance of graphitic carbon nitride photocatalyst

Graphitic carbon nitride (gCN or $g-C_3N_4$) is an outstanding photocatalyst that has gained popularity in the photodegradation of dyes due to its superior performance in photocatalysis activity. The $g-C_3N_4$ absorbs solar photons for conversion into chemical energy resulting in the degradation of dyes into harmless compounds [53]. The

Table 2
Summary of synthesized GO-based photocatalyst for dye removal

Material	Target compound	Highlights	Removal capacity (%)	Reference
Co/Ni/GO	MO	Modified composite photocatalyst exhibited higher degradation efficiency compared to pristine GO due to the enhancement of charge transfer of GO.	84% removal efficiency of MO.	[73]
G-ZnO	RhB MB MO	Photodegradation of RhB has observed the highest degradation rate.	100% removal efficiency of RhB, MB and MO.	[76]
GO-CdSe	CR	CdSe incorporation has significantly improved the photodegradation efficiency of CR with 100% removal of 20 ppm of CR within 10 min.	100% removal efficiency of CR.	[77]
Graphene oxide/SnO_2	RhB MB	When SnO_2-GO nanocomposites are used as photoanode material for photoelectric conversion, appropriate doping of GO is also beneficial to improve the intensity and stability of photocurrent.	SnO_2 0.1% GO showed removal of RhB (97.26%) and MB (89.43%) degradation within 90 min (2 ppm initial concentration).	[79]
V_2O_5 nanorods/graphene oxide	Victoria blue dye (VB)	Decoration of V_2O_5 nanorods on the surface of GO has made the nanocomposite a suitable visible light-sensitive material.	GO-V_2O_5 exhibited almost 100% degradation of VB dye within just 90 min (10 ppm initial concentration).	[78]
Graphene oxide reinforced bismuth titanate (GO/BT)	Direct blue 15 (DB15)	BT's reflectance decreased in the visible region after the addition of GO caused higher light absorption in the visible region and enhanced the photocatalytic activity of BT.	5% GO substituted bismuth titanate degrades the DB15 1% within 3 h (50 ppm initial concentration).	[80]
GO/MIL-101(Fe)/ PANCMA	RhB	Enhancement of RhB removal was due to the formation of heterostructures and more active surface reaction sites due to GO and MIL-101(Fe).	100% RhB removal after 30 min under visible light.	[81]
ZnO/GO	Methyl red (MR)	High values of photocatalytic efficiency of the ZnO-GNc may be due to the improved charge passage and separation.	ZnO-GNc with 5 wt.% GO achieved removal of MR at ~98.12% under visible light.	[82]
GO-TiO_2	Orange ME2RL	GO-TiO_2 nanocomposite effective for the treatment of organic azo dye.	99.6% at the first cycle of Orange ME2RL removal (100 ppm initial concentration).	[83]
Polyaniline/dicarboxyl acid cellulose-GO	Reactive brilliant red K-2G	Simultaneous adsorption-photocatalysis process effectively removed brilliant red K-2G.	Almost 100% when the initial concentration was (0.1 ppm).	[84]
GO nanosheets	MB	GO nanosheets provide desired redox reaction and enhance the light-harvesting.	60% removal of MB.	[75]

combination of two semiconductors to form a heterojunction for the proper transport of excited charges, including the two neighbouring semiconductors' proper band structures, have become a great alternative to improve the performance of g-C_3N_4 against dye degradation. g-C_3N_4 can be derived by thermal condensation of various low-cost nitrogen-rich precursors without direct C–C bonding such as cyanamide [85], dicyandiamide [86], melamine [87], thiourea [88], urea [24] or mixtures. However, the bulky g-C_3N_4 produced from these routes usually will result in a very low surface area up to below 10 m² g⁻¹. Only by using the topotactical template does the surface area of bulk g-C_3N_4 increase to 60–80 m² g⁻¹ [89]. Compared with mesoporous g-C_3N_4, the surface area is relatively higher than bulk g-C_3N_4 which can be up to 350 m² g⁻¹. Mesoporous g-C_3N_4, usually abbreviated as (mp g-C_3N_4), can be obtained with an established process of mesostructured material by hard templating or nano-casting by replication of silica sphere or mesoporous silica objects. This method basically involves filling or coating a rigid template with a precursor material and further treatment of the precursor to become the desired material, followed by removing the template to create a replica. Emerging development on g-C_3N_4 structure modifications focuses on producing GCN nanosheets and thin films. Inspired by the huge achievement of graphene exfoliated from bulk graphite, a sonication-assisted liquid-exfoliation was successfully prepared a thin layer of g-C_3N_4 nanosheets (2D) from bulk GCN (3D) with surface area as high as 384 m² g⁻¹ [90–92]. The high surface area of GCN facilitates the good mass transfer and accommodates more active sites for reactions at the surface.

Yong et al. [93] constructed a floating photocatalyst from the polyetherimide (PEI) and graphitic carbon nitride via a hydrothermal assisted ultra-sonication method. The PEI solution was mixed with the g-C_3N_4 powder in a centrifuge tube, and then the mixture was ultrasonicated and shaken for 30 min. The floating photocatalyst was tested on the Methyl orange (MO) as a sampling material for photodegradation of the PEI-g-C_3N_4 reaction. The result shows that the PEI act as a linker for the PEI-g-C_3N_4 composite while g-C_3N_4 contribute to the photodegradation of MO. The mechanical motion such as stirring affect the photodegradation efficiency as if a stirring is applied for pure g-C_3N_4, the efficiency is 11% higher than PEI-gC_3N_4. However, if the stirring is not being applied, the photodegradation efficiency of pure graphitic is lower than the obtained photocatalyst. The floating mechanism of photocatalyst adds merit to the catalyst since most photocatalyst is in powder form. It enables them to utilize more sunlight energy as they float on the surface of wastewater and carry their reaction.

Ben Abdelaziz et al. [94] previously introduced Bi_2O_3 as a suitable electron platform to accept the photogenerated electrons from g-C_3N_4. When irradiated under visible light, the composite showed the degradation of RhB dyes excellently. The induction of excited charges from g-C_3N_4 to BiOl with the CB position of BiOl is well below the CB of g-C_3N_4. Thus, possesses enough potential to drive the degradation of RhB dye. Besides coupling two semiconductors, forming a Z-scheme system can also improve the charge separation of g-C_3N_4. The excited electrons and holes belonging to two semiconductors move across the hetero-junctional interface to combine. From this way, the photogenerated electrons in the CB of one photocatalyst and holes in the valence band (VB) of the other photocatalyst are well separated and thus enhance the photocatalytic activities.

Wang et al. [95] successfully synthesize the Z-scheme Bismuth vanadate/porous graphitic carbon nitride (BiVO₄/Pg-C_3N_4) composite through a hydrothermal process, operating at 180°C for 24 h. He proposed this Z-scheme mechanism due to the charge density of Pg-C_3N_4 being higher than the BiVO₄. Therefore, the excessive electron from the interface of Pg-C_3N_4 will flow to the surface of BiVO₄. When the photogenerated electrons on CB of BiVO₄ are transferred to an interface, the electrons will migrate to VB Pg-C_3N_4 to recombine with holes, thus resulting in a beneficial boosting of the holes on VB BiVO₄. Therefore, the electrons on CB of Pg-C_3N_4 will migrate to the BiVO₄ surface to participate in the photocatalytic reaction. This way, a strong redox capability under visible light was achieved using the Z-scheme mechanism.

In other cases, Jia et al. [55] developed composite graphitic carbon nitride photocatalyst through the heterogeneous Z-scheme method by using $SnFe_2O_4$ as the $SnFe_3O_4$ is more negative charge than the g-C_3N_4 in the redox reaction sites. The transmission electron microscopy (TEM) results confirm the formation of composite structure as it detects the crumpled structural layer that indicates the C and N element of the g-C_3N_4, and it also detects the $SnFe_3O_4$ nanostructure with the sizes of 100–200 nm. The closed contact of g-C_3N_4/$SnFe_3O_4$ inhibits the charge recombination of electron-hole pair as the lifetime emission of gC_3N_4 is much longer when it is introduced to $SnFe_3O_4$. According to Jia et al. [55], the longer the emission lifetime, the higher the separation efficiency of electron-hole pair as the photogenerated recombination rate reduced. Furthermore, the outstanding performance of g-C_3N_4 based composite photocatalyst was demonstrated by Sujubili et al. [32], synthesized Fe_3O_4@SiO_2@g-C_3N_4/TiO_2 composite photocatalyst from core-shell structure method. The examination on the photoluminescence intensity, the weight ratio, and the UV Vis analysis of composite revealed that the optimum photocatalytic activity was achieved at a ratio of 15 wt.% of g-C_3N_4/TiO_2@Fe_3O_4@SiO_2 with the optimum condition of 2.08 eV band gap and 50,000 a.u. intensity, respectively. The integrated magnetic material in the composite help to increase the regeneration rate of the composite and thus pro-long the lifespan of the photocatalyst. The Fe_3O_4@SiO_2@g-C_3N_4/TiO_2 can be regenerated twice after degrading the RhB under sunlight irradiation over 3 h.

Table 3 shows the performance based on the g-C_3N_4 material, and based on the result, the removal efficiency for magnetic photocatalyst is more than 90%. Furthermore, the material embedded with the photocatalysts did not reduce the photocatalytic performance of the photocatalyst, instead of improving their performance. In short, similar to GO composite photocatalyst, the photocatalytic performance of g-C_3N_4 can be boosted either by being modified with magnetic material or doping with other excellent materials such as semiconductor materials, carbon materials, and noble materials metals and nanoparticles. Table 3 summarises the example of synthesized graphitic carbon nitride-based photocatalyst for dyes removal.

Table 3
Summary of synthesized graphitic carbon nitride-based photocatalyst for dye removal
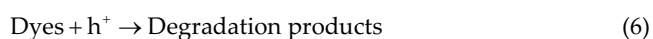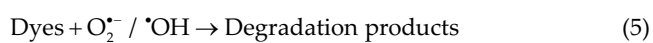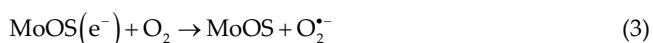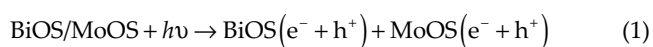
Material	Target compound	Highlights	Removal capacity (%)	Reference
Fe_3O_4@SiO_2@g-C_3N_4/TiO_2	RhB MO	Band gap value of Fe_3O_4@SiO_2@g-C_3N_4/TiO_2 composite is directly proportional to the ratio of g-C_3N_4 (2.5 eV at 5% wt. to 2.82 eV at 20% wt. of g-C_3N_4). This band gap enhanced the visible light region's absorption, thus leading to increased photocatalytic activity.	91% removal efficiency of RhB and MO.	[32]
g-C_3N_4/Fe_3O_4/Ag/ Ag_2SO_3	RhB	Absorption bands of the g-C_3N_4/Fe_3O_4/Ag/Ag_2SO_3 NP decreased in comparison to the pure g-C_3N_4 (470 to 450 nm).	99% removal efficiency of RhB within 270 min.	[96]
g-C_3N_4/Fe_3O_4/ Ag_3PO_4/Co_3O_4	MB RhB MO	With the presence of Co_3O_4, the degradation rate of RhB under light irradiation increased from 360 to 150 min.	85.7% removal efficiency of RhB within 360 min while 95% removal efficiency of MO within 150 min.	[97]
Laiwu iron ore (LW)/graphitic carbon nitride (g-C_3N_4/LW)	MB	LW particle distributed more evenly on the g-C_3N_4 nanosheets as the amount of g-C_3N_4 increased. It escalates the number of reactive sites on the photocatalyst's surface, thus providing a better photocatalytic activity.	97% removal efficiency of MB within 60 min.	[35]
Thin-layer boron-doped graphitic carbon nitride nanosheets (B-g-C_3N_4)	Eosin Y RhB MB MO	Thin-layer B-g-C_3N_4 nanosheets have much higher photocatalytic activity and can be used for visible light driven degrading various organic dyes.	Eosin Y, RhB, MB, MO 100% degraded within 5, 10, 20 and 60 min respectively under visible light irradiation.	[98]
Water dispersible g-C_3N_4	MB	N-rich g-C_3N_4 precursors strongly influenced the photocatalytic activities for bulk g-C_3N_4. In addition, the presence of foreign atoms (sulfur, S) in thiourea induced the formation of sulfur-containing nanoporous water-dispersible g-C_3N_4.	Highest removal MB capacity is observed for TCp (q_e = 277.45 mg/g) (thiourea).	[99]
g-C_3N_4/PAN nanofiber	MB	Synergetic effects of concentration and degradation of MB species are the important factors for the high photodegradation efficiency of MB.	Effective photocatalytic activity confirmed by 97.3% degradation of MB under visible light irradiation.	[50]
g-C_3N_4@C, N co-doped	MO	Simultaneous formation of multicomponent heterojunction with core-shell structure provided an enormous impact in designing highly active photocatalyst with superior interfacial charge transfer.	gT500 sample with the degradation percentage of 95.0% after 3.5 h.	[23]
Trace samarium-doped graphitic carbon nitride	Metanil yellow (MY)	pH is a very important parameter amongst other variables for the effective degradation and removal of MY from wastewater.	93% and 87% were removed within 6 h using samarium-doped g-C_3N_4 at pH 3 and 6.4, respectively.	[100]
Cerium ion adsorbed graphitic carbon nitride	MB	g-C_3N_4 decorated cerium increased specific surface areas to give more active sites for extended visible light absorption, improved electronic structures for efficient charge transfer, reduced the recombination probability of photogenerated charge carriers.	Efficiency removal of MC up to 95% and 56% in water under sunlight and visible irradiation, respectively.	[101]

4.3. Performance of molybdenum disulfide (MoS$_2$) photocatalyst

Molybdenum disulfide (MoS$_2$) has recently received attention as a visible-light responsive component for the degradation of dyes and photocatalytic evolution of hydrogen, H$_2$ due to its high mobility of charge carriers and excellent optical absorption property. The unique layered MoS$_2$ consists of molybdenum atoms sandwiched between two hexagonally close-packed sulfur atoms, enabling alkaline metal ions to be intercalated or deintercalated through the interlayers, making it a suitable candidate for dye degradation. MoS$_2$ often undergoes modification before being used as the photocatalyst for the photodegradation of dyes. In particular, it will combine with other semiconductors with the band gap value lower than MoS$_2$ to increase their light-responsive ability and minimalize the electron-recombination potential.

Chen et al. [59] previously developed the magnetic MoS$_2$ by intercalating it with zinc-aluminium hydrotalcite and testing it to degrade MB. The result of his work showed that the maximum degradation of Methylene blue dye reached up to 93% within 30 min of adsorption and 150 min of photo illumination. Besides that, under the morphological characterization, the scanning electron microscopy (SEM) shows the particle size of MoS$_2$ is reduced because of the interlaminar structure of hydrotalcite. Therefore, it increased the photocatalytic performance of MoS$_2$. In addition, to remove the polluted dyes from the wastewater, Fekadu et al. [102] have study on the performance of Bi$_2$(O, S)$_3$/Mo(OS)$_2$ composite photocatalyst for the degradation of 4 different types of dyes, and it fabricated through a facile method. The stability and reusability of photocatalyst have been examined, and it has shown that the photodegradation of MB and RhB dyes has slightly dropped after the third run.

Moreover, the efficiency of photodegradation activity decreased due to the mass loss of the photocatalyst surface after the washing procedure. Therefore, to avoid this, the photocatalyst has been immobilized into or onto suitable adsorbents such as carbon or PAN fibre. The reaction mechanism steps of the BiOS/MoOS composite are shown in Eqs. (1)–(6) [102]:

$$BiOS/MoOS + h\upsilon \rightarrow BiOS\left(e^- + h^+\right) + MoOS\left(e^- + h^+\right) \tag{1}$$

$$BiOS\left(e^-\right) + MoOS\left(h^+\right) \rightarrow BiOS + MoOS \tag{2}$$

$$MoOS\left(e^-\right) + O_2 \rightarrow MoOS + O_2^{\bullet-} \tag{3}$$

$$O_2^{\bullet-} + 2H^+ \rightarrow 2^{\bullet}OH \tag{4}$$

$$Dyes + O_2^{\bullet-} / {}^{\bullet}OH \rightarrow Degradation\ products \tag{5}$$

$$Dyes + h^+ \rightarrow Degradation\ products \tag{6}$$

Following the result of the photoluminescence (PL) analysis made by Zeng et al. [103], the recombination rate of photoinduced electron–hole pairs of the MoS$_2$/CoFe$_2$O$_4$ (M/C) composites at the excitation wavelength of 375 nm is lesser than the pure MoS$_2$ and CoFe$_2$O$_4$ as the emission intensity of the M/C composite is much lower than both of MoS$_2$ and CoFe$_2$O$_4$. In addition, the Z scheme heterojunction mechanism of the M/C composite enhanced the PL electron–hole between the CoFe$_2$O$_4$, which act as the photogenerated electron at the conduction band (CB), with the MoS$_2$, that will generate a photogenerated hole at the valence band (VB). As a consequence, the degradation efficiency of RhB and CR by the M/C composite is high due to the presence of active species which are O$_2^{\bullet}$ and holes.

Based on Table 4, the modified MoS$_2$ is an excellent candidate as a semiconductor photocatalyst for the degradation of various dyes through photocatalytic activity [59,102–105]. The efficiency removal of Rhodium B dye from the solution reaction by the modified molybdenum disulfide is mostly higher than 90%, indicating that this photocatalyst is favourable in eliminating the cationic dyes from the polluted water. Besides that, with the combination of photocatalyst with other materials, the modified molybdenum disulfide has improved its regeneration ability and be easily separated from the contaminated solution. Table 4 tabulates the summary of synthesized graphitic carbon nitride-based photocatalyst for dye removal.

5. Future trends and challenges

The heterogeneous composite photocatalyst can be a promising material for water remediation because of its good physicochemical properties and excellent electronic structure stability. Furthermore, the functionality of the photocatalyst can be enhanced through modification with other materials like noble metals, nanoparticles, semiconductors, magnetic and carbon materials as it upgrades the efficiency and recyclability of the photocatalyst. Upgrading the recyclability of photocatalyst add a merit point to the photocatalyst as it is a significant factor that determines the cost-effectiveness and the longevity of the photocatalyst performance. However, based on the currently available data, more fundamental research is needed to establish a stable composite photocatalyst technology to treat large volumes of industrial dye wastewater and prolonged operation.

First and foremost, the research scientists need to focus on synthesizing the composite photocatalyst through a green method, and it must be environmentally friendly. Furthermore, they need to balance the photocatalyst's recovery rate with the magnetic particle's agglomeration rate as the nanomaterials tend to agglomerate due to Van der Waals force. Furthermore, the corrosion factor should be considered in future research for the composite photocatalyst to be practically applicable in real-time conditions. In the future, photocatalyst's design or synthesis should focus on photocatalyst with a slower reaction time to optimize the applicability of photocatalyst in real-time conditions. Last but not least, for future trends, more exploration needs to be done on the composite photocatalyst, which focuses on dye removal in wastewater.

Table 4
Summary of synthesized molybdenum disulfide based photocatalyst for dye removal

Photocatalyst	Target compound	Highlights	Removal capacity (%)	Reference
MoS_2/ZnAl-LDH composite	MB	Excessive amount of composite caused the photocatalytic degradation efficiency to decrease. Based on the degradation curve, the best amount of photocatalyst is 40 mg.	93% removal efficiency of MB.	[59]
$Bi_2(O,S)_3$/ $Mo(O,S)_2$	MO RhB MB	Absorption peak of all dyes substantially decreased with the presence of composite. The highest recorded time for the degradation of the targeted compound is 180 min, Methylene blue.	96% removal efficiency of MO and RhB while 98% removal efficiency of MB.	[102]
Fe_3O_4@MoS_2/ Ag_3PO_4 (FM/A)	Congo red (CR) RhB	Specific surface area of the (FM/A) composite has increased to 76.56 m^2, thus allowing the composite to produce more active sites for the photocatalytic reaction.	90% removal efficiency of CR while 98% removal efficiency of RhB.	[104]
Fe_3O_4/TiO_2/MoS_2	RhB	Sample from the X-ray diffraction analysis confirmed that the MoS_2 is in the 2H structural type (hexagonal type), which is a stable structure for the formation of the magnetic photocatalyst.	98% removal efficiency of RhB.	[105]
MoS_2/$CoFe_2O_4$ composites	RhB CR	According to the TEM analysis, the mass ratio of MoS_2 and $CoFe_2O_4$ has dramatically impacted the photocatalytic degradation activity. The best ratio for the degradation activity is 1:3 of $CoFe_2O_4$ to MoS_2.	93% removal efficiency of RhB while 94% removal efficiency of CR.	[103]
Lyophilized tin-doped MoS_2	RhB	Excellent photocatalytic activity of DL-MoS_2 due to accelerated electron transfer upon Sn doping and fast generated electron–hole pair because of a higher surface area.	100% degradation RhB within 30 min with 10 ppm initial concentration.	[106]
Layered MoS_2	MB Crystal violet (CV)	Enhanced photocatalytic MB and CV dye degradation might be due to the high energy of UV light as compared to natural sunlight.	MoS_2 degrades almost 71% and 57% of MoS_2-MB and MoS_2-CV, respectively, within 90 min under natural sunlight. Under the artificial lamps, the degradation was 82% and 73% of MoS_2-MB and MoS_2-CV, respectively, within 90 min.	[107]
MoS_2 nanosheets	CV	Dye degradation was observed as a decrease in absorbance of the dye with a time under the solar irradiation in the presence of MoS_2 NSs.	0.1 g/L MoS_2 degradation of 40 μM CV dye under solar irradiation within 50 min with degradation efficiency and the kinetic rate constant were 92% and 0.049 min^{-1}.	[108]

(Continued)

Table 4 Continued

Photocatalyst	Target compound	Highlights	Removal capacity (%)	Reference
MoS_2-TiO_2@PAN nanofiber	MB	Large surface area of MoS_2 nanosheets ensured sufficient active sites whereby TiO_2 nano-tubes could act as spacers to isolate MoS_2 nanosheets and further increase the surface area and active sites of MoS_2 nanosheets. The matched band gaps between MoS_2 and TiO_2 provided efficient electron transfer performance.	Best degradation efficiency of the as-prepared MoS_2-TiO_2@PAN membrane was 97.73% on MB.	[109]
Flowerlike MoS_2/ $SrFe_{12}O_{19}$	MB	Exposed interface region of the p–n heterojunction formed by $SrFe_{12}O_{19}$/ MoS_2 can reduce the recombination rate of the photogenerated electron–hole pairs, thus effectively improving the charge transfer rate and accelerating photoinduced charge carrier separation.	$SrFe_{12}O_{19}$/MoS_2 composite achieved 97% degradation rate for MB under visible light with 20 ppm initial concentration within 125 min.	[110]

6. Conclusions

In conclusion, dye degradation in wastewater can be achieved through efficient photocatalytic activity. This review highlights the emerging photocatalyst materials that have been widely used in dye wastewater remediation. Moreover, the general information on the type of photocatalysts type of dyes, the performance of photocatalysts and significant findings from the research works were included in this review. Overall, enhanced photocatalytic activity on dyes was due to various plausible reasons. Depending on the operating conditions of the photocatalysis process, the performance of dye removal was due to excellent morphological, physicochemical and thermal properties of photocatalysts, light adsorption, narrow energy band gap, high specific surface area, and low electron-hole pair recombination rate of the photocatalysts. Therefore, myriad research work have been done to develop a composite photocatalyst instead of a bare photocatalyst. In this review, made photocatalyst based graphene oxide (GO), graphitic carbon nitride (g-C_3N_4), and molybdenum disulfide (MoS_2) for photodegradation of dyes have been summarised. The composite photocatalyst processes pose an outstanding performance to become a potential candidate for dye wastewater treatment due to their excellent performance in removing dyes with low toxicity levels. Moreover, it can be readily used or incorporated into different forms to improve its recyclability. However, the application of photocatalyst for the treatment of industrial dye wastewater scale needs major attention as the photocatalyst used needs to be environmentally friendly, applicable in mass production, high recyclability and high corrosion resistance.

Acknowledgement

References

[1] O.A. Shabaan, H.S. Jahin, G.G. Mohamed, Removal of anionic and cationic dyes from wastewater by adsorption using multiwall carbon nanotubes, Arabian J. Chem., 13 (2020) 4797–4810.

[2] J. Mateo-Sagasta, S.M. Zadeh, H. Turral, J. Burke, Water Pollution From Agriculture: A Global Review, Executive Summary, UN-Water Family News, 2017.

[3] United Nations World Water Assessment Programme, World Water Development Report, Wastewater: The Untapped Resource, 2017. Available at: https://doi.org/10.1017/CBO9781107415324.004

[4] C.N.C. Hitam, A.A. Jalil, A review on exploration of Fe_2O_3 photocatalyst towards degradation of dyes and organic contaminants, J. Environ. Manage., 258 (2020) 110050, doi: 10.1016/j.jenvman.2019.110050.

[5] T.A. Nguyen, R.S. Juang, Treatment of waters and wastewaters containing sulfur dyes: a review, Chem. Eng. J., 219 (2013) 109–117.

[6] Y. Tang, M. Li, C. Mu, J. Zhou, B. Shi, Ultrafast and efficient removal of anionic dyes from wastewater by polyethyleneimine-modified silica nanoparticles, Chemosphere, 229 (2019) 570–579.

[7] S. Jorfi, G. Barzegar, M. Ahmadi, R. Darvishi Cheshmeh Soltani, N. Alah Jafarzadeh Haghighifard, A. Takdastan, R. Saeedi, M. Abtahi, Enhanced coagulation-photocatalytic treatment of Acid red 73 dye and real textile wastewater using UVA/synthesized MgO nanoparticles, J. Environ. Manage., 177 (2016) 111–118.

[8] S.L. Chan, Y.P. Tan, A.H. Abdullah, S.T. Ong, Equilibrium, kinetic and thermodynamic studies of a new potential

biosorbent for the removal of Basic blue 3 and Congo red dyes: pineapple (*Ananas comosus*) plant stem, J. Taiwan Inst. Chem. Eng., 61 (2016) 306–315.

[9] S. Benkhaya, S. M' rabet, A. El Harfi, A review on classifications, recent synthesis and applications of textile dyes, Inorg. Chem. Commun., 115 (2020) 107891, doi: 10.1016/j.inoche.2020.107891.

[10] D. Wen, W. Li, J. Lv, Z. Qiang, M. Li, Methylene blue degradation by the VUV/UV/persulfate process: effect of pH on the roles of photolysis and oxidation, J. Hazard. Mater., 391 (2020) 121855, doi: 10.1016/j.jhazmat.2019.121855.

[11] B. Chen, Y. Liu, S. Chen, X. Zhao, X. Meng, X. Pan, Magnetically recoverable cross-linked polyethylenimine as a novel adsorbent for removal of anionic dyes with different structures from aqueous solution, J. Taiwan Inst. Chem. Eng., 67 (2016) 191–201.

[12] Z. Lü, F. Hu, H. Li, X. Zhang, S. Yu, M. Liu, C. Gao, Composite nanofiltration membrane with asymmetric selective separation layer for enhanced separation efficiency to anionic dye aqueous solution, J. Hazard. Mater., 368 (2019) 436–443.

[13] X. Wu, D. Zhang, F. Jiao, S. Wang, Visible-light-driven photodegradation of Methyl orange using $Cu_2O/ZnAl$ calcined layered double hydroxides as photocatalysts, Colloids Surf., A, 508 (2016) 110–116.

[14] K. Zhou, X.Y. Hu, B.Y. Chen, C.C. Hsueh, Q. Zhang, J. Wang, Y.J. Lin, C.T. Chang, Synthesized $TiO_2/ZSM-5$ composites used for the photocatalytic degradation of azo dye: intermediates, reaction pathway, mechanism and bio-toxicity, Appl. Surf. Sci., 383 (2016) 300–309.

[15] C. Lv, S. Chen, Y. Xie, Z. Wei, L. Chen, J. Bao, C. He, W. Zhao, S. Sun, C. Zhao, Positively-charged polyethersulfone nanofibrous membranes for bacteria and anionic dyes removal, J. Colloid Interface Sci., 556 (2019) 492–502.

[16] M. Ikram, S. Ali, M. Aqeel, A. Ul-hamid, Reduced graphene oxide nanosheets doped by Cu with highly efficient visible light photocatalytic behavior, J. Alloys Compd., 837 (2020) 155588, doi: 10.1016/j.jallcom.2020.155588.

[17] A.P. Angelika Tkaczyk, K. Mitrowska, Synthetic organic dyes as contaminants of the aquatic environment and their implications for ecosystems: a review, Sci. Total Environ., 717 (2019) 137222, doi: 10.1016/j.scitotenv.2020.137222.

[18] A.L. Desa, N.H.H. Hairom, L.Y. Ng, C.Y. Ng, M.K. Ahmad, A.W. Mohammad, Industrial textile wastewater treatment via membrane photocatalytic reactor (MPR) in the presence of ZnO-PEG nanoparticles and tight ultrafiltration, J. Water Process Eng., 31 (2019) 100872, doi: 10.1016/j.jwpe.2019.100872.

[19] A. Khosravi, M. Karimi, H. Ebrahimi, N. Fallah, Sequencing batch reactor/nanofiltration hybrid method for water recovery from textile wastewater contained phthalocyanine dye and anionic surfactant, J. Environ. Chem. Eng., 8 (2020) 103701, doi: 10.1016/j.jece.2020.103701.

[20] S. Hube, M. Eskafi, K.F. Hrafnkelsdóttir, B. Bjarnadóttir, M.Á. Bjarnadóttir, S. Axelsdóttir, B. Wu, Direct membrane filtration for wastewater treatment and resource recovery: a review, Sci. Total Environ., 710 (2020) 136375, doi: 10.1016/j.scitotenv.2019.136375.

[21] Z. Chang, Y. Chen, S. Tang, J. Yang, Y. Chen, S. Chen, P. Li, Z. Yang, Construction of chitosan/polyacrylate/graphene oxide composite physical hydrogel by semi-dissolution/acidification/sol–gel transition method and its simultaneous cationic and anionic dye adsorption properties, Carbohydr. Polym., 229 (2020) 115431, doi: 10.1016/j.carbpol.2019.115431.

[22] N.H. Alias, J. Jaafar, S. Samitsu, T. Matsuura, A.F. Ismail, M.H.D. Othman, M.A. Rahman, N.H. Othman, N. Abdullah, S.H. Paiman, N. Yusof, F. Aziz, Photocatalytic nanofiber-coated alumina hollow fiber membranes for highly efficient oilfield produced water treatment, Chem. Eng. J., 360 (2019) 1437–1446.

[23] M.A. Mohamed, J. Jaafar, M.F.M. Zain, L.J. Minggu, M.B. Kassim, M.S. Rosmi, N.H. Alias, N.A.M. Nor, W.N.W. Salleh, M.H.D. Othman, In-depth understanding of core-shell nanoarchitecture evolution of $g-C_3N_4@C,N$ co-doped anatase/rutile: efficient charge separation and enhanced visible-light photocatalytic performance, Appl. Surf. Sci., 436 (2018) 302–318.

[24] N.H. Alias, J. Jaafar, S. Samitsu, N. Yusof, M.H.D. Othman, M.A. Rahman, A.F. Ismail, F. Aziz, W.N.W. Salleh, N.H. Othman, Photocatalytic degradation of oilfield produced water using graphitic carbon nitride embedded in electrospun polyacrylonitrile nanofibers, Chemosphere, 204 (2018) 79–86.

[25] N.M. Viet, D.Q. Trung, B.L. Giang, N.L.M. Tri, P. Thao, T.H. Pham, F.Z. Kamand, T.M. Al Tahtamouni, Noble metal-doped graphitic carbon nitride photocatalyst for enhancement photocatalytic decomposition of antibiotic pollutant in wastewater under visible light, J. Water Process Eng., 32 (2019) 100954, doi: 10.1016/j.jwpe.2019.100954.

[26] J. You, Y. Guo, R. Guo, X. Liu, A review of visible light-active photocatalysts for water disinfection: features and prospects, Chem. Eng. J., 373 (2019) 624–641.

[27] M. Xiao, B. Luo, S. Wang, L. Wang, Solar energy conversion on $g-C_3N_4$ photocatalyst: light harvesting, charge separation, and surface kinetics, J. Energy Chem., 27 (2018) 1111–1123.

[28] W. Wang, G. Huang, J.C. Yu, P.K. Wong, Advances in photocatalytic disinfection of bacteria: development of photocatalysts and mechanisms, J. Environ. Sci. (China), 34 (2015) 232–247.

[29] D. Maučec, A. Šuligoj, A. Ristić, G. Dražić, A. Pintar, N.N. Tušar, Titania versus zinc oxide nanoparticles on mesoporous silica supports as photocatalysts for removal of dyes from wastewater at neutral pH, Catal. Today, 310 (2018) 32–41.

[30] A. Fujishima, T.N. Rao, D.A. Tryk, Titanium dioxide photocatalysis, J. Photochem. Photobiol., C, 1 (2000) 1–21.

[31] A. Fouda, S.S. Salem, A.R. Wassel, M.F. Hamza, T.I. Shaheen, Optimization of green biosynthesized visible light active CuO/ZnO nano-photocatalysts for the degradation of organic Methylene blue dye, Heliyon, 6 (2020) 1–13.

[32] S. Narzary, K. Alamelu, V. Raja, B.M.J. Ali, Visible light active, magnetically retrievable $Fe_3O_4@SiO_2@g-C_3N_4/TiO_2$ nanocomposite as efficient photocatalyst for removal of dye pollutants, J. Environ. Chem. Eng., 8 (2020) 1–9.

[33] R. Ma, S. Zhang, T. Wen, P. Gu, L. Li, G. Zhao, F. Niu, Q. Huang, Z. Tang, X. Wang, A critical review on visible-light-response CeO_2-based photocatalysts with enhanced photooxidation of organic pollutants, Catal. Today, 335 (2019) 20–30.

[34] A. Sudhaik, P. Raizada, P. Shandilya, P. Singh, Magnetically recoverable graphitic carbon nitride and $NiFe_2O_4$ based magnetic photocatalyst for degradation of oxytetracycline antibiotic in simulated wastewater under solar light, J. Environ. Chem. Eng., 6 (2018) 3874–3883.

[35] Q. Zhou, F. Peng, Y. Ni, J. Kou, C. Lu, Long afterglow phosphor driven round-the-clock $g-C_3N_4$ photocatalyst, J. Photochem. Photobiol., A, 328 (2016) 182–188.

[36] A.V. Karim, A. Selvaraj, Graphene composites in photocatalytic oxidation of aqueous organic contaminants – a state of art, Process Saf. Environ. Prot., 146 (2021) 136–160.

[37] C. Min, Y. Mo, K. Kim, D. Wang, C. Su, Y. Yoon, Chemosphere potential utility of graphene-based nano spinel ferrites as adsorbent and photocatalyst for removing organic/inorganic contaminants from aqueous solutions: a mini review, Chemosphere, 221 (2019) 392–402.

[38] A.T. Smith, A.M. LaChance, S. Zeng, B. Liu, L. Sun, Synthesis, properties, and applications of graphene oxide/reduced graphene oxide and their nanocomposites, Nano Mater. Sci., 1 (2019) 31–47.

[39] M. Pedrosa, E.S. Da Silva, L.M. Pastrana-Martínez, G. Drazic, P. Falaras, J.L. Faria, J.L. Figueiredo, A.M.T. Silva, Hummers' and Brodie's graphene oxides as photocatalysts for phenol degradation, J. Colloid Interface Sci., 567 (2020) 243–255.

[40] N.F.D. Junaidi, N.H. Othman, M.Z. Shahruddin, N.H. Alias, F. Marpani, W. Lau, A.F. Ismail, Fabrication and characterization of grahene-polyethersulfne (GO-PES) composite flat sheet and hollow fiber membranes for oil-water separation, J. Chem. Technol. Biotechnol., 95 (2020) 1308–1320.

[41] N.F.D. Junaidi, N.A. Khalil, A.F. Jahari, N.Z.K. Shaari, M.Z. Shahruddin, N.H. Alias, N.H. Othman, Effect of graphene

oxide (GO) on the surface morphology & hydrophilicity of polyethersulfone (PES), IOP Conf. Ser.: Mater. Sci. Eng., 358 (2018) 12047, http://stacks.iop.org/1757-899X/358/i=1/a=012047.

[42] N.H. Othman, N.H. Alias, M.Z. Shahruddin, N.F. Abu Bakar, N.R. Nik Him, W.J. Lau, Adsorption kinetics of Methylene blue dyes onto magnetic graphene oxide, J. Environ. Chem. Eng., 6 (2018) 2803–2811.

[43] N.H. Othman, N.H. Alias, M.Z. Shahruddin, S.N.C.M. Hussein, A. Dollah, Supported graphene oxide hollow fibre membrane for oily wastewater treatment, AIP Conf. Proc., 1901 (2017) 020008, doi: 10.1063/1.5010445.

[44] N.H. Othman, A.F. Jahari, N.H. Alias, Demulsification of crude oil in water (O/W) emulsions using graphene oxide demulsification of crude oil in water (O/W) emulsions using graphene oxide, IOP Conf. Ser.: Mater. Sci. Eng., 458 (2018) 012023, doi: 10.1088/1757-899X/458/1/012023.

[45] C. Prasad, Q. Liu, H. Tang, G. Yuvaraja, J. Long, A. Rammohan, G.V. Zyryanov, An overview of graphene oxide supported semiconductors based photocatalysts: properties, synthesis and photocatalytic applications, J. Mol. Liq., 297 (2020) 111826, doi: 10.1016/j.molliq.2019.111826.

[46] A.T. Lawal, Graphene-based nano composites and their applications. A review, Biosens. Bioelectron., 141 (2019) 111384, doi: 10.1016/j.bios.2019.111384.

[47] Q. Hu, E. Rezaee, H. Shan, P. Liu, Z.X. Xu, Graphene oxide/N-CuMe$_2$Pc nanorod hybrid nanocomposite as efficient visible light photocatalyst for aqueous Cr(VI) reduction, Catal. Today, 335 (2019) 180–186.

[48] M. Nadimi, A. Ziarati Saravani, M.A. Aroon, A. Ebrahimian Pirbazari, Photodegradation of Methylene blue by a ternary magnetic TiO$_2$/Fe$_3$O$_4$/graphene oxide nanocomposite under visible light, Mater. Chem. Phys., 225 (2019) 464–474.

[49] N. Le Minh Tri, J. Kim, B.L. Giang, T.M. Al Tahtamouni, P.T. Huong, C. Lee, N.M. Viet, D. Quang Trung, Ag-doped graphitic carbon nitride photocatalyst with remarkably enhanced photocatalytic activity towards antibiotic in hospital wastewater under solar light, J. Ind. Eng. Chem., 80 (2019) 597–605.

[50] N.H. Alias, J. Jaafar, S. Samitsu, A.F. Ismail, N.A.M. Nor, N. Yusof, F. Aziz, Mechanistic insight of the formation of visible-light responsive nanosheet graphitic carbon nitride embedded polyacrylonitrile nanofibres for wastewater treatment, J. Water Process Eng., 33 (2020) 101015, doi: 10.1016/j.jwpe.2019.101015.

[51] N.H. Alias, J. Jaafar, S. Samitsu, T. Matsuura, A.F. Ismail, S. Huda, N. Yusof, F. Aziz, Photocatalytic nanofiber-coated alumina hollow fiber membranes for highly efficient oilfield produced water treatment, Chem. Eng. J., 360 (2019) 1437–1446.

[52] N.H. Alias, J. Jaafar, S. Samitsu, A.F. Ismail, M.H.D. Othman, M.A. Rahman, N.H. Othman, N. Yusof, F. Aziz, T.A.T. Mohd, Efficient removal of partially hydrolysed polyacrylamide in polymer-flooding produced water using photocatalytic graphitic carbon nitride nanofibres, Arabian J. Chem., 13 (2020) 4341–4349.

[53] M. Baca, W. Kukułka, K. Cendrowski, E. Mijowska, R.J. Kaleńczuk, B. Zielińska, Graphitic carbon nitride and titanium dioxide modified with 1 D and 2 D carbon structures for photocatalysis, ChemSusChem, 12 (2019) 612–620.

[54] M. Chegeni, Z. Mousavi, M. Soleymani, S. Dehdashtian, Removal of aspirin from aqueous solutions using graphitic carbon nitride nanosheet: theoretical and experimental studies, Diamond Relat. Mater., 101 (2020) 107621, doi: 10.1016/j.diamond.2019.107621.

[55] Y. Jia, H. Ma, W. Zhang, G. Zhu, W. Yang, N. Son, M. Kang, C. Liu, Z-scheme SnFe$_2$O$_4$-graphitic carbon nitride: reusable, magnetic catalysts for enhanced photocatalytic CO$_2$ reduction, Chem. Eng. J., 383 (2020) 123172, doi: 10.1016/j.cej.2019.123172.

[56] X. Li, J. Xiong, X. Gao, J. Huang, Z. Feng, Z. Chen, Y. Zhu, Recent advances in 3D g-C$_3$N$_4$ composite photocatalysts for photocatalytic water splitting, degradation of pollutants and CO$_2$ reduction, J. Alloys Compd., 802 (2019) 196–209.

[57] J. Zhao, Y. Liu, Y. Wang, H. Li, J. Wang, Z. Li, Boron-doped graphitic carbon nitride dots dispersed on graphitic carbon nitride/graphene hybrid nanosheets as high performance photocatalysts for hydrogen evolution reaction, Appl. Surf. Sci. J., 470 (2019) 923–932.

[58] V. Hasija, P. Raizada, V.K. Thakur, A.A. Parwaz Khan, A.M. Asiri, P. Singh, An overview of strategies for enhancement in photocatalytic oxidative ability of MoS$_2$ for water purification, J. Environ. Chem. Eng., 8 (2020) 1–21.

[59] S. Chen, F. Yang, Z. Cao, C. Yu, S. Wang, H. Zhong, Enhanced photocatalytic activity of molybdenum disulfide by compositing ZnAl–LDH, Colloids Surf., A, 586 (2020) 124140, doi: 10.1016/j.colsurfa.2019.124140.

[60] M. Zhao, Z. Ye, R. Suzuki, Y. Ye, H.Y. Zhu, J. Xiao, Y. Wang, Y. Iwasa, X. Zhang, Atomically phase-matched second-harmonic generation in a 2D crystal, Light Sci. Appl., 5 (2016) 1–6.

[61] K. Sun, F. Jia, B. Yang, C. Lin, X. Li, S. Song, Synergistic effect in the reduction of Cr(VI) with Ag-MoS$_2$ as photocatalyst, Appl. Mater. Today, 18 (2020) 100453, doi: 10.1016/j.apmt.2019.100453.

[62] M. Al Kausor, D. Chakrabortty, Graphene oxide-based semiconductor photocatalysts for degradation of organic dye in wastewater: a review on fabrication, performance enhancement and challenges, Inorg. Chem. Commun., 129 (2021) 108630, doi: 10.1016/J.INOCHE.2021.108630.

[63] Z. Tong, D. Yang, J. Shi, Y. Nan, Y. Sun, Z. Jiang, Three-dimensional porous aerogel constructed by g-C$_3$N$_4$ and graphene oxide nanosheets with excellent visible-light photocatalytic performance, ACS Appl. Mater. Interfaces, 7 (2015) 25693–25701.

[64] E. Suvaci, E. Özel, Hydrothermal Synthesis, M. Pomeroy, Ed., Encyclopedia of Materials: Technical Ceramics and Glasses, Elsevier, Amsterdam, Netherlands, 2021, pp. 59–68.

[65] O. Akhavan, Graphene nanomesh by ZnO nanorod photocatalysts, ACS Nano, 4 (2010) 4174–4180.

[66] M. Hong Wu, L. Li, Y. Cheng Xue, G. Xu, L. Tang, N. Liu, W. Yuan Huang, Fabrication of ternary GO/g-C$_3$N$_4$/MoS$_2$ flower-like heterojunctions with enhanced photocatalytic activity for water remediation, Appl. Catal., B, 228 (2018) 103–112.

[67] I. Ahmad, S. Shukrullah, M. Ahmad, E. Ahmed, M.Y. Naz, M.S. Akhtar, N.R. Khalid, A. Hussain, I. Hussain, Effect of Al doping on the photocatalytic activity of ZnO nanoparticles decorated on CNTs and graphene: solvothermal synthesis and study of experimental parameters, Mater. Sci. Semicond. Process., 123 (2021) 105584, doi: 10.1016/J.MSSP.2020.105584.

[68] B.G. Rao, D. Mukherjee, B.M. Reddy, Chapter 1 – Novel approaches for preparation of nanoparticles, D. Ficai, A.M. Grumezescu, Ed., Nanostructures for Novel Therapy: Synthesis, Characterization and Applications Micro and Nano Technologies, Elsevier, Amsterdam, Netherlands, 2017, pp. 1–36.

[69] W.-K. Jo, N.Clament Sagaya Selvam, Enhanced visible light-driven photocatalytic performance of ZnO-g-C$_3$N$_4$ coupled with graphene oxide as a novel ternary nanocomposite, J. Hazard. Mater., 299 (2015) 462–470.

[70] J. Yan, Z. Song, X. Wang, Y. Xu, W. Pu, H. Xu, S. Yuan, H. Li, Enhanced photocatalytic activity of ternary Ag$_3$PO$_4$/GO/g-C$_3$N$_4$ photocatalysts for Rhodamine B degradation under visible light radiation, Appl. Surf. Sci., 466 (2019) 70–77.

[71] M.B. Gawande, S.N. Shelke, R. Zboril, R.S. Varma, Microwave-assisted chemistry: synthetic applications for rapid assembly of nanomaterials and organics, Acc. Chem. Res., 47 (2014) 1338–1348.

[72] K.-Y. Shih, Y.-L. Kuan, E.-R. Wang, One-step microwave-assisted synthesis and visible-light photocatalytic activity enhancement of BiOBr/RGO nanocomposites for degradation of Methylene blue, Materials (Basel), 14 (2021) 4577, doi: 10.3390/MA14164577.

[73] F. Khurshid, M. Jeyavelan, S. Nagarajan, Photocatalytic dye degradation by graphene oxide doped transition metal catalysts, Synth. Met., 278 (2021) 116832, doi: 10.1016/J.SYNTHMET.2021.116832.

[74] S. Kumar, A. Kumar, Chemically derived luminescent graphene oxide nanosheets and its sunlight driven photocatalytic activity

against Methylene blue dye, Opt. Mater. (Amst), 62 (2016) 320–327.

[75] K. Govindan, A.K. Suresh, T. Sakthivel, K. Murugesan, R. Mohan, V. Gunasekaran, A. Jang, Effect of peroxomonosulfate, peroxodisulfate and hydrogen peroxide on graphene oxide photocatalytic performances in Methyl orange dye degradation, Chemosphere, 237 (2019) 124479, doi: 10.1016/J.CHEMOSPHERE.2019.124479.

[76] M. Maruthupandy, P. Qin, T. Muneeswaran, G. Rajivgandhi, F. Quero, J.M. Song, Graphene-zinc oxide nanocomposites (G-ZnO NCs): synthesis, characterization and their photocatalytic degradation of dye molecules, Mater. Sci. Eng. B, 254 (2020) 114516, doi: 10.1016/J.MSEB.2020.114516.

[77] S. Das, P. Somu, S. Paul, Visible light induced efficient photocatalytic degradation of azo dye into nontoxic byproducts by CdSe quantum dot conjugated nano graphene oxide, J. Mol. Liq., 340 (2021) 117055, doi: 10.1016/J.MOLLIQ.2021.117055.

[78] M. Beaula Ruby Kamalam, S.S.R. Inbanathan, K. Sethuraman, A. Umar, H. Algadi, A.A. Ibrahim, Q.I. Rahman, C.S. Garoufalis, S. Baskoutas, Direct sunlight-driven enhanced photocatalytic performance of V_2O_5 nanorods/graphene oxide nanocomposites for the degradation of Victoria blue dye, Environ. Res., 199 (2021) 111369, doi: 10.1016/j.envres.2021.111369.

[79] Z. Fu, B. Qin, X. Guo, Y. Wang, Y. Xu, Q. Qiao, Q. Wang, F. Wang, S. Gao, Z. Yang, Enhancement of photocatalytic dye degradation and photoconversion capacity of graphene oxide/SnO_2 nanocomposites, J. Alloys Compd, 898 (2022) 162796, doi: 10.1016/j.jallcom.2003.10.002.

[80] D. Sivaraj, K. Vijayalakshmi, M. Srinivasan, P. Ramasamy, Graphene oxide reinforced bismuth titanate for photocatalytic degradation of azo dye (DB15) prepared by hydrothermal method, Ceram. Int., 47 (2021) 25074–25080.

[81] Z. Huang, Z. Lai, D. Zhu, H. Wang, C. Zhao, G. Ruan, F. Du, Electrospun graphene oxide/MIL-101(Fe)/poly(acrylonitrile-co-maleic acid) nanofiber: a high-efficient and reusable integrated photocatalytic adsorbents for removal of dye pollutant from water samples, J. Colloid Interface Sci., 597 (2021) 196–205.

[82] F. Anjum, A.M. Asiri, M.A. Khan, M.I. Khan, S.B. Khan, K. Akhtar, E.M. Bakhsh, K.A. Alamry, S.Y. Alfifi, S. Chakraborty, Photo-degradation, thermodynamic and kinetic study of carcinogenic dyes via zinc oxide/graphene oxide nanocomposites, J. Mater. Res. Technol., 15 (2021) 3171–3191.

[83] V. Kumaran, P. Sudhagar, A.K. Konga, G. Ponniah, Photocatalytic Degradation of synthetic organic reactive dye wastewater using GO-TiO_2 nanocomposite, Polish J. Environ. Stud., 29 (2020) 1683–1690.

[84] T. Liu, Z. Wang, X. Wang, G. Yang, Y. Liu, Adsorption-photocatalysis performance of polyaniline/dicarboxyl acid cellulose@graphene oxide for dye removal, Int. J. Biol. Macromol., 182 (2021) 492–501.

[85] S.S. Park, S.-W. Chu, C. Xue, D. Zhao, C.-S. Ha, Facile synthesis of mesoporous carbon nitrides using the incipient wetness method and the application as hydrogen adsorbent, J. Mater. Chem., 21 (2011) 10801, doi: 10.1039/c1jm10849b.

[86] G. Wu, Y. Hu, Y. Liu, J. Zhao, X. Chen, V. Whoehling, C. Plesse, G.T.M. Nguyen, F. Vidal, W. Chen, Graphitic carbon nitride nanosheet electrode-based high-performance ionic actuator, Nat. Commun., 6 (2015), doi: 10.1038/ncomms8258.

[87] J. Fang, H. Fan, M. Li, C. Long, Nitrogen self-doped graphitic carbon nitride as efficient visible light photocatalyst for hydrogen evolution, J. Mater. Chem. A, 3 (2015) 13819–13826.

[88] Y.-Q. Dong, M. Wang, L. Chen, M.-J. Li, Preparation, characterization of P(VDF-HFP)/[bmim]BF_4 ionic liquids hybrid membranes and their pervaporation performance for ethyl acetate recovery from water, Desalination, 295 (2012) 53–60.

[89] Y.S. Jun, E.Z. Lee, X. Wang, W.H. Hong, G.D. Stucky, A. Thomas, From melamine-cyanuric acid supramolecular aggregates to carbon nitride hollow spheres, Adv. Funct. Mater., 23 (2013) 3661–3667.

[90] P. Niu, L. Zhang, G. Liu, H. Cheng, Graphene-like carbon nitride nanosheets for improved photocatalytic activities, Adv. Funct. Mater., 22 (2012) 4763–4770.

[91] S. Yang, Y. Gong, J. Zhang, L. Zhan, L. Ma, Z. Fang, X. Wang, P.M. Ajayan, Exfoliated graphitic carbon nitride nanosheets as efficient catalysts for hydrogen evolution under visible light, J. Adv. Mater., 25 (2013) 2452–2456.

[92] T. Xu, F. Wu, Y. Gu, Y. Chen, J. Cai, W. Lu, H. Hu, Z. Zhu, W. Chen, Visible-light responsive electrospun nanofibers based on polyacrylonitrile-dispersed graphitic carbon nitride, RSC Adv., 5 (2015) 86505–86512.

[93] Y. Guo, R. Wang, P. Wang, Y. Li, C. Wang, Developing polyetherimide/graphitic carbon nitride floating photocatalyst with good photodegradation performance of Methyl orange under light irradiation, Chemosphere, 179 (2017) 84–91.

[94] M. Ben Abdelaziz, B. Chouchene, L. Balan, T. Gries, G. Medjahdi, H. Ezzaouia, R. Schneider, One pot synthesis of bismuth oxide/graphitic carbon nitride composites with high photocatalytic activity, Mol. Catal., 463 (2019) 110–118.

[95] Z. Wang, J. Lv, J. Zhang, K. Dai, C. Liang, Facile synthesis of Z-scheme $BiVO_4$/porous graphite carbon nitride heterojunction for enhanced visible-light-driven photocatalyst, Appl. Surf. Sci., 430 (2018) 595–602.

[96] M.J. Lima, M.J. Sampaio, C.G. Silva, A.M.T. Silva, J.L. Faria, Magnetically recoverable Fe_3O_4/g-C_3N_4 composite for photocatalytic production of benzaldehyde under UV-LED radiation, Catal. Today, 328 (2019) 293–299.

[97] M. Mousavi, A. Habibi-yangjeh, Novel magnetically separable g-C_3N_4/Fe_3O_4/Ag_3PO_4/Co_3O_4 nanocomposites: visible-light-driven photocatalysts with highly enhanced activity, Adv. Powder Technol., 28 (2017) 1540–1553.

[98] Y. Zhong, Y. Lin, Q. Chen, Y. Sun, F.F. Fu, Rapid photo-degradation of various organic dyes with thin-layer boron-doped graphitic carbon nitride nano-sheets under visible light irradiation, J. Environ. Chem. Eng., 8 (2020) 103567, doi: 10.1016/j.jece.2019.103567.

[99] T.K.A. Nguyen, T.T. Pham, H. Nguyen-Phu, E.W. Shin, The effect of graphitic carbon nitride precursors on the photocatalytic dye degradation of water-dispersible graphitic carbon nitride photocatalysts, Appl. Surf. Sci., 537 (2021) 148027, doi: 10.1016/j.apsusc.2020.148027.

[100] N. Masunga, B.B. Mamba, K.K. Kefeni, Trace samarium doped graphitic carbon nitride photocatalytic activity toward Metanil yellow dye degradation under visible light irradiation, Colloids Surf., A, 602 (2020) 125107, doi: 10.1016/j.colsurfa.2020.125107.

[101] S.K. Kuila, R. Sarkar, P. Kumbhakar, P. Kumbhakar, C.S. Tiwary, T.K. Kundu, Photocatalytic dye degradation under sunlight irradiation using cerium ion adsorbed two-dimensional graphitic carbon nitride, J. Environ. Chem. Eng., 8 (2020) 103942, doi: 10.1016/j.jece.2020.103942.

[102] F.T. Bekena, D.H. Kuo, W.L. Kebede, Universal and highly efficient degradation performance of novel $Bi_2(O,S)_3$/$Mo(O,S)_2$ nanocomposite photocatalyst under visible light, Sep. Purif. Technol., 247 (2020) 117042, doi: 10.1016/j.seppur.2020.117042.

[103] Y. Zeng, N. Guo, Y. Song, Y. Zhao, H. Li, X. Xu, J. Qiu, H. Yu, Fabrication of Z-scheme magnetic MoS_2/$CoFe_2O_4$ nanocomposites with highly efficient photocatalytic activity, J. Colloid Interface Sci., 514 (2018) 664–674.

[104] N. Guo, H. Li, X. Xu, H. Yu, Hierarchical Fe_3O_4@MoS_2/Ag_3PO_4 magnetic nanocomposites: enhanced and stable photocatalytic performance for water purification under visible light irradiation, Appl. Surf. Sci., 389 (2016) 227–239.

[105] Y. Sun, J. Tan, H. Lin, X. Wang, J. Liu, Y. Li, C. Wang, A facile strategy for the synthesis of ferroferric oxide/titanium dioxide/molybdenum disulfide heterostructures as a magnetically separable photocatalyst under visible-light, J. Colloid Interface Sci., 516 (2018) 138–144.

[106] P. Nandigana, M. Sanchayan, D. Manjubashini, P. Basudev, B. Subramanian, S.K. Panda, Lyophilized tin-doped MoS_2 as an efficient photocatalyst for overall degradation of Rhodamine B dye, J. Alloys Compd., 907 (2022) 164470, doi: 10.1016/j.jallcom.2005.05.002.

[107] D. Gawari, V. Pandit, N. Jawale, P. Kamble, Layered MoS_2 for photocatalytic dye degradation, Mater. Today Proc., 53 (2022) 10–14.

[108] P. Sharma, M.K. Singh, M.S. Mehata, Sunlight-driven MoS_2 nanosheets mediated degradation of dye (Crystal violet) for wastewater treatment, J. Mol. Struct., 1249 (2022) 131651, doi: 10.1016/j.molstruc.2021.131651.

[109] X. Zhang, K. Fu, Z. Su, Fabrication of 3D MoS_2-TiO_2@ PAN electro-spun membrane for efficient and recyclable photocatalytic degradation of organic dyes, Mater. Sci. Eng., B, 269 (2021) 115179, doi: 10.1016/j.mseb.2021.115179.

[110] S. Chen, Y. Di, H. Li, M. Wang, B. Jia, R. Xu, X. Liu, Efficient photocatalytic dye degradation by flowerlike MoS_2/$SrFe_{12}O_{19}$ heterojunction under visible light, Appl. Surf. Sci., 559 (2021) 149855, doi: 10.1016/j.apsusc.2021.149855.